OLD DOMINION UNIVERSITY RESEARCH FOUNDATION

DEPARTMENT OF PHYSICS AND GEOPHYSICAL SCIENCES
SCHOOL OF SCIENCES AND HEALTH PROFESSIONS
OLD DOMINION UNIVERSITY
NORFOLK, VIRGINIA

Technical Report PGSTR-AP77-47

A THEORETICAL/EXPERIMENTAL PROGRAM TO DEVELOP ACTIVE OPTICAL POLLUTION SENSORS

Prepared by

Frank S. Mills

and

Roger N. Blais

Earl C. Kindle, Principal Investigator

Final Report

Prepared for the
National Aeronautics and Space Administration
Langley Research Center
Hampton, Virginia

Under
Research Grant NSG 1060
Ellis E. Remsberg, Technical Monitor
Lidar Applications Section

January 1977

DEPARTMENT OF PHYSICS AND GEOPHYSICAL SCIENCES
SCHOOL OF SCIENCES AND HEALTH PROFESSIONS
OLD DOMINION UNIVERSITY
NORFOLK, VIRGINIA

Technical Report PGSTR-AP77-47

A THEORETICAL/EXPERIMENTAL PROGRAM TO DEVELOP ACTIVE OPTICAL POLLUTION SENSORS

Prepared by

Frank S. Mills

and

Roger N. Blais

Earl C. Kindle, Principal Investigator

Final Report

Prepared for the
National Aeronautics and Space Administration
Langley Research Center
Hampton, Virginia 23665

Under
Research Grant NSG 1060
Ellis E. Remsberg, Technical Monitor
Lidar Applications Section

Submitted by the
Old Dominion University Research Foundation
Norfolk, Virginia 23508

January 1977

A THEORETICAL/EXPERIMENTAL PROGRAM TO DEVELOP ACTIVE OPTICAL POLLUTION SENSORS

By

Frank S. Mills[1] and Roger N. Blais[2]

I. Introduction

The intent of this research project was to develop and apply Light Detection and Ranging (LIDAR) technology to the assessment of air quality, and to evaluate its usefulness by actual field tests. Necessary hardware, to be described below (Section 3Aii) was successfully constructed and operated in the field. Measurements of necessary physical parameters, such as SO_2 absorption coefficients were successfully completed, and theoretical predictions of differential absorption performance were reported. Plume modeling improvements were proposed (cf. appendix). A full scale field test of equipment, data analysis and auxiliary data support was conducted in Maryland during September 1976. Thus, significant strides were made in all four areas (system development and demonstration; theoretical; field measurements; and modeling) described in the work statement of the original proposal.

The following report will briefly summarize work previously reported, and then describe in detail the recent development in the work of Old Dominion University personnel both at Langley Research Center and on the Norfolk campus.

---

[1] Research Associate, Old Dominion University Research Foundation, Norfolk, Virginia 23508.

[2] Assistant Professor, Department of Physics and Geophysical Sciences, Old Dominion University, Norfolk, Virginia 23508.

II. Work Previously Reported

Material included in progress reports will be outlined here, but not reproduced. Three reports dated respectively June 6, 1975; October, 1975; and December, 1975 were submitted.

The June 6, 1975 report covered four basic topics reported in detailed appendices. First, a report on "Measurements of SO_2 Absorption Coefficients Using a Tunable Dye Laser" by R. T. Thompson, Jr., J. M. Hoell, Jr., and W. R. Wade. Absorption coefficients for the 3001.8 Å, 2981.0 Å and 2962 Å centered electronic-vibrational transitions were reported with a wavelength uncertainty of +0.1 Å. Next, a report on "Remote Sensing of Atmospheric SO_2 Using the Differential Absorption Lidar Technique" by Hoell, Wade and Thompson was included. Results from a computer simulation of a DIAL system indicated that commercially available technology could achieve measurement sensitivities less than 2 ppb with spatial resolution of 500 m over ranges of less than 2 km. Third, Thompson reported "Sensitivity Predictions for Differential Absorption and Scattering Lidar." General statistical error analysis equations were developed for analyzing the sensitivity of a DAS system, and they were evaluated for three experimental situations: ground level nitrogen dioxide (NO_2) measurements over a horizontal path; measurements of ozone (O_3) depletion in jet engine wakes at 20 km altitude; and orbiting platform, nadir viewing

atmospheric ozone distribution measurements. Finally, Thompson and F. Allario reported on "Optical Properties of Tunable Diode Laser Radiation," in which divergence, polarization and pattern anomalies in the far field pattern of tunable dye lasers were investigated.

The October, 1975 report (Technical Report PGSTR-PH75-12) by S. K. Poultney, M. L. Brumfield and J. S. Siviter was subtitled Quantitative Remote Raman Lidar Measurements of Pollutants from Stationary Sources. A detailed study of using Raman lidar was conducted using a calibration tank at LaRC. It was shown that typical stack exit concentrations of 500 ppm SO_2 could be measured to an accuracy of 10 percent at a distance of 300 m, with integration times of 30 minutes.

The December, 1975 report by R. T. Thompson, Jr., "Differential Absorption and Scattering Sensitivity Predictions" was a much fuller account of the studies summarized in the June 6 report.

III. Work Previously Unreported

Included below are results previously unreported. Section A consists of work done by ODU personnel at LaRC, and it is divided into two subsections, the first theoretical and the second experimental. It is the work of Dr. Mills and his group. Section B contains a brief description of various activities of ODU personnel working on campus. A fuller presentation of their results is found in the appendix.

A. Work Done At Langley Research Center

i) Theoretical Support for the NASA Langley Water Vapor DIAL Experiment.

The purpose of the experiment was to demonstrate the feasibility of the differential absorption lidar technique for measuring water vapor profiles in the troposphere up to 3 km. For optimum operation the technique should use water vapor lines which are relatively isolated in frequency, have an absorption cross-section which is relatively insensitive to changes in temperature, and have an absorption cross-section which is large enough to produce measurable absorption, but not large enough to completely absorb the laser radiation. The work described here involves determining what water vapor lines would be least sensitive to temperature changes.

Assuming an isolated Lorentz shaped absorption line, the following expression for the absorption coefficient, k', may be written.

$$k' = \frac{S\ \gamma}{\pi(\Delta\nu^2 + \gamma^2)} \tag{1}$$

where S is the line strength, γ is the Lorentz half-width, and $\Delta\nu$ is the difference between the frequency of interest and the frequency of the absorption line. Both the line strength S and Lorentz half-width γ are temperature dependent. The half-width temperature dependence can be expressed by the following expression.

$$\gamma = \gamma_0 \left(\frac{T_0}{T}\right)^{\frac{1}{2}} \tag{2}$$

where γ_0 is the defined as the half-width at temperature T_0 and T is the temperature. The temperature dependence of the line strength can be expressed as follows:

$$S = K_0\ T^{-3/2}\ e^{-hcE/kT} \tag{3}$$

where K_0 is a constant, T is the temperature, h is Planck's constant, c is the speed of light, k is Boltzmann's constant, and E is the energy of the lower energy level of the transition expressed as wave number.

The dye laser used in the DIAL experiment has a line width which is comparable to the absorption line width. Therefore, the absorption which is measured by the DIAL is the absorption integrated over the laser line width. The approach used

here will be to calculate the integrated absorption assuming some laser line shape, and then determine for a given temperature the lower state energy for which the integrated absorption is least sensitive to temperature variations.

Calculations were made for two different laser line shapes, square and triangular. The actual laser line shape is somewhere in between. Let $F(\nu')$ be a function describing the laser line shape where

$$\int_{-\infty}^{\infty} F(\nu')\, d\nu' = 1 \quad . \tag{4}$$

Figure 1 shows the two laser line shapes graphically.

For the square line shape $F(\nu')$ may be written

$$F(\nu') = 1/2w \qquad -w < \nu' < w \tag{5}$$
$$F(\nu') = 0 \qquad |\nu'| > w$$

For the triangular line shape $F(\nu')$ may be written

$$F(\nu') = 1/2w - \nu'/4w^2 \qquad 0 \leq \nu' < 2w \tag{6}$$
$$F(\nu') = 1/2w + \nu'/4w^2 \qquad -2w < \nu' \leq 0$$
$$F(\nu') = 0 \qquad |\nu'| > 2w$$

For the square laser line shape, the integrated absorption k' is

$$k' = 2\int_{0}^{w} \frac{S \cdot \gamma \ (1/2w)}{\pi(\nu'^2 + \gamma^2)}\, d\nu' \tag{7}$$

or

$$k' = (S/w\pi) \tan^{-1}(w/\gamma) \tag{8}$$

For the triangular laser line shape, the integrated absorption k' is

$$k' = 2\int_0^{2w} \frac{S\ \gamma\ (1/2w - \nu'/4w^2)}{\pi(\nu'^2 + \gamma^2)}\, d\nu' \qquad (9)$$

or

$$k' = (S\gamma/\pi w)\left[(1/\gamma)\tan^{-1}(2w/\gamma) - (1/4w)\ln\ (1 + 4w^2/\gamma^2)\right] \qquad (10)$$

Now, for each laser line shape the temperature dependence of S and γ from equations 2 and 3 can be substituted into the expressions for the integrated absorption, and the lower state energy for temperature insensitive lines can be calculated by taking the derivative of the integrated absorption with respect to temperature, setting the derivative equal to zero and solving for E.

Following the procedure described above for a square laser line, the integrated absorption k' in equation 8 can be written

$$k' = \frac{K_0 T^{-3/2}}{w\pi}\ e^{-hcE/kT}\ \tan^{-1}\ \left(\frac{wT^{\frac{1}{2}}}{\gamma_0 T_0^{\frac{1}{2}}}\right) \qquad (11)$$

or

$$k' = K'T^{-3/2}e^{-hcE/kT}\tan^{-1}(wT^{\frac{1}{2}}/\gamma_0 T_0^{\frac{1}{2}}) \qquad (12)$$

where

$$K' = K_0/w\pi \quad . \qquad (13)$$

Taking the derivative of equation (12) with respect to T

$$\frac{dk'}{dT} = K'T^{-2}e^{-hcE/kT}\left[\frac{hcE}{kT}\,T^{-\frac{1}{2}}\tan^{-1}\left(\frac{wT^{\frac{1}{2}}}{\gamma_0 T_0^{\frac{1}{2}}}\right) - \frac{3}{2}\,T^{-\frac{1}{2}}\tan^{-1}\left(\frac{wT^{\frac{1}{2}}}{\gamma_0 T_0^{\frac{1}{2}}}\right) + \frac{w}{2\gamma_0 T_0^{\frac{1}{2}}\left(1+\frac{w^2T}{\gamma_0^2 T_0}\right)}\right]. \tag{14}$$

For temperature insensitive lines $\frac{dk'}{dT} = 0$.

$$\frac{hcE}{kT}\,T^{-\frac{1}{2}}\tan^{-1}\left(\frac{wT^{\frac{1}{2}}}{\gamma_0 T_0^{\frac{1}{2}}}\right) - \frac{3}{2}\,T^{-\frac{1}{2}}\tan^{-1}\left(\frac{wT^{\frac{1}{2}}}{\gamma_0 T_0^{\frac{1}{2}}}\right) + \frac{w}{2\gamma_0 T_0^{\frac{1}{2}}\left(1+\frac{w^2T}{\gamma_0^2 T_0}\right)} = 0 \tag{15}$$

or

$$\frac{hcE}{kT}\,\tan^{-1}\left(\frac{wT^{\frac{1}{2}}}{\gamma_0 T_0^{\frac{1}{2}}}\right) = \frac{3}{2}\,\tan^{-1}\left(\frac{wT^{\frac{1}{2}}}{\gamma_0 T_0^{\frac{1}{2}}}\right) - \frac{wT^{\frac{1}{2}}}{2\gamma_0 T_0^{\frac{1}{2}}\left(1+\frac{w^2T}{\gamma_0^2 T_0}\right)}. \tag{16}$$

Solving for E

$$E = \frac{kT}{hc}\left[\frac{3}{2} - \frac{wT^{\frac{1}{2}}}{2\gamma_0 T_0^{\frac{1}{2}}\left(1+\frac{w^2T}{\gamma_0^2 T_0}\right)\tan^{-1}\left(\frac{wT^{\frac{1}{2}}}{\gamma_0 T_0^{\frac{1}{2}}}\right)}\right]. \tag{17}$$

Following the same procedures for the triangular laser line, the integrated absorption k' in equation (10) can be written

$$k' = \frac{K_0\gamma_0 T_0^{\frac{1}{2}}T^{-2}}{\pi w}\,e^{-hcE/kT}\left[\frac{1T^{\frac{1}{2}}}{\gamma_0 T_0^{\frac{1}{2}}}\,\tan^{-1}\left(\frac{2wT^{\frac{1}{2}}}{\gamma_0 T_0^{\frac{1}{2}}}\right) - \frac{1}{4w}\ln\left(1+\frac{4w^2T}{\gamma_0^2 T_0}\right)\right] \tag{18}$$

or

$$k' = K'T^{-3/2}e^{-hcE/kT}\tan^{-1}\left(\frac{2wT^{\frac{1}{2}}}{\gamma_0 T_0^{\frac{1}{2}}}\right) - \frac{K'}{4w}\gamma_0 T_0^{\frac{1}{2}}T^{-2}e^{(-hcE/kT)}\ln\left(1+\frac{4w^2T}{\gamma_0^2 T_0}\right) \quad (19)$$

where

$$K' = \frac{K_0}{\pi w} . \quad (20)$$

Taking the derivative of equation 19 with respect to T

$$\frac{dk'}{dT} = K'e^{(-hcE/kT)}T^{-5/2}\left[\frac{hcE}{kT}\tan^{-1}\left(\frac{2wT^{\frac{1}{2}}}{\gamma_0 T_0^{\frac{1}{2}}}\right) - \frac{3}{2}\tan^{-1}\left(\frac{2wT^{\frac{1}{2}}}{\gamma_0 T_0^{\frac{1}{2}}}\right) + \frac{wT^{\frac{1}{2}}}{\gamma_0 T_0^{\frac{1}{2}}\left(1+\frac{4w^2T}{\gamma_0^2 T_0}\right)}\right]$$

$$- \frac{K'}{4w}\gamma_0 T_0^{\frac{1}{2}}e^{-hcE/kT}T^{-3}\left[\frac{hcE}{kT}\ln\left(1+\frac{4w^2T}{\gamma_0^2 T_0}\right) - 2\ln\left(1+\frac{4w^2T}{\gamma_0^2 T_0}\right) + \frac{4w^2T}{\gamma_0^2 T_0\left(1+\frac{4w^2T}{\gamma_0^2 T_0}\right)}\right] \quad (21)$$

For temperature insensitive lines $\frac{dk'}{dT} = 0$

$$\frac{hcE}{kT}\tan^{-1}\left(\frac{2wT^{\frac{1}{2}}}{\gamma_0 T_0^{\frac{1}{2}}}\right) - \frac{3}{2}\tan^{-1}\left(\frac{2wT^{\frac{1}{2}}}{\gamma_0 T_0^{\frac{1}{2}}}\right) = \frac{hcE}{kT}\frac{\gamma_0 T_0^{\frac{1}{2}}}{4w\pi^{\frac{1}{2}}}\ln\left(1+\frac{4w^2T}{\gamma_0^2 T_0}\right) - \frac{\gamma_0 T_0^{\frac{1}{2}}}{2wT^{\frac{1}{2}}}\ln\left(1+\frac{4w^2T}{\gamma_0^2 T_0}\right) \quad (22)$$

or

$$\frac{hcE}{kT}\left[\tan^{-1}\left(\frac{2wT^{\frac{1}{2}}}{\gamma_0 T_0^{\frac{1}{2}}}\right) - \frac{\gamma_0 T_0^{\frac{1}{2}}}{4wT^{\frac{1}{2}}}\ln\left(1+\frac{4w^2T}{\gamma_0^2 T_0}\right)\right]$$

$$= \frac{3}{2}\tan^{-1}\left(\frac{2wT^{\frac{1}{2}}}{\gamma_0 T_0^{\frac{1}{2}}}\right) - \frac{\gamma_0 T_0^{\frac{1}{2}}}{2wT^{\frac{1}{2}}}\ln\left(1+\frac{4w^2T}{\gamma_0^2 T_0}\right) \qquad (23)$$

or

$$E = \frac{kT}{hc}\left[\frac{3}{2} - \frac{\frac{\gamma_0 T_0^{\frac{1}{2}}}{8wT^{\frac{1}{2}}}\ln\left(1+\frac{4w^2T}{\gamma_0^2 T_0}\right)}{\tan^{-1}\left(\frac{2wT^{\frac{1}{2}}}{\gamma_0 T_0^{\frac{1}{2}}}\right) - \frac{\gamma_0 T_0^{\frac{1}{2}}}{4wT^{\frac{1}{2}}}\ln\left(1+\frac{4w^2T}{\gamma_0^2 T_0}\right)}\right] \qquad (24)$$

A sample calculation will be made for each laser line shape assuming that w, the laser line half-width and γ_0, the absorption line half-width, are equal, and that $T = T_0 = 296K$. For the square line shape using equation 17, the result is

$$E = 1.18\,\frac{kT}{hc} = 243\ cm^{-1} \qquad (25)$$

For the triangular line shape using equation 24, the result is

$$E = 1.21\,\frac{kT}{hc} = 249\ cm^{-1}. \qquad (26)$$

The results of the sample calculations indicate that if the laser line width is comparable to the absorption line width the lower state energy for temperature insensitive lines is relatively independent of the exact laser line shape.

Using a procedure similar to that outlined above, it can be shown that for a monochromatic laser line, the lower state energy for temperature insensitive absorption lines is just kT/hc or for T = 396K, 206 cm^{-1}. Thus, the fact that the

laser line has a finite width has more effect on determining the lower state energy for temperature insensitive lines than the exact shape of the laser line.

ii) Analysis of the DIAL Technique for Remote Probing of SO_2 in the Atmosphere

SO_2 from fossil fuel powerplants is one of the primary problems contributing to degradation of regional air quality in this country. It is, therefore, desirable to develop remote sensing techniques which can monitor SO_2 emissions from stationary sources or ambient SO_2 concentration in an urban environment. Poultney, et al.[1], have reported the results of an experimental program to determine the usefulness of the Raman lidar as a technique for remotely monitoring SO_2 emissions from fossil fuel powerplants. In this report, currently available SO_2 spectra are used to predict the performance of the Differential Absorption Lidar (DIAL) technique operating near 4 μm and 300 nm for remote sensing of SO_2 in the atmosphere. These two wavelength regions are covered by lasers which NASA Langley Research Center currently has under development.

The DIAL concept can be described qualitatively as follows. Pulsed laser radiation at two wavelengths is transmitted into the atmosphere. The two wavelengths are selected so that one, called the on wavelength, is absorbed by the gas of interest and the other, called the off wavelength, is not. The backscatter return signal as a function

of range at each wavelength is collected by an optical receiver. Now define a range cell as the distance from R_1 to R_2. The average concentration of the absorbing gas in the range cell may be determined from the on and off wavelength returns at R_1 and R_2. The situation is analagous to a dual-beam spectroscopy experiment where the off wavelength return corresponds to the reference beam, the on wavelength corresponds to the sample beam, and the range cell corresponds to the sample cell. The transmittance of the absorbing gas in the range cell is then just the ratio of the on wavelength returns at R_2 and R_1 divided by the ratio of the off wavelength returns at R_2 and R_1.

The quantitative expression for absorber concentration can be found using the lidar equation:

$$P_r(R,\lambda,t) = K \frac{L}{2} \frac{A}{R^2} P_0(\lambda)\ \beta\ (R,\lambda,t)$$

$$\times \exp\{-2\int_0^R [\alpha_{sc}(r,\lambda,t) + N_A(r,t)\sigma_A(\lambda,P,T)$$

$$+ N_{int}(r,t)\sigma_{int}(\lambda,P,T)]\, dr\}. \qquad (27)$$

Here P_r is the received power as a function of range R, wavelength λ, and time t; K is a constant; L is the laser pulse length; A is the receiver area; $P_0(\lambda)$, the transmitted power, is a function of wavelength; β is the backscatter cross section as a function of range, wavelength, and time; α_{sc} is the extinction coefficient for scattering as a function

of range, wavelength and time; N_A is the concentration of the absorbing gas of interest as a function of range and time; σ_A is the absorption cross section of the gas of interest as a function of wavelength, pressure, P, and temperature, T; N_{int} is concentration of any interfering absorbing gas; and σ_{int} is the absorption cross section of the interfering gas.

A number of assumptions are made to simplify the analysis. The scattering terms are assumed equal for the on wavelength and the off wavelength returns, that is $\beta(R,\lambda off,t\ off) = \beta(R,\lambda on,t\ on)$ and $\alpha_{sc}(R,\lambda off,\ t\ off) = \alpha_{sc}(R,\lambda on,t\ on)$. Also, the concentrations of the absorbing and interfering gases are assumed to remain constant between the off wavelength and on wavelength returns, that is, $N_A(R,t\ off) = N_A(R,t\ on)$ and $N_{int}(R,t\ off) = N_{int}(R,t\ on)$. The on and off wavelength absorption cross section for the gas of interest, $\sigma_A(\lambda off,P,T)$ and $\sigma_A(\lambda on,P,T)$, are assumed to be known and constant between R_1 and R_2. If $\sigma_{int}(\lambda off,P,T)$ is not equal to $\sigma_{int}(\lambda on,P,T)$, then both the concentration and absorption cross section of the interfering gas must be known or must be determined by a separate experiment.

With the above assumptions the average concentration N_A of the gas of interest in the range cell between R_1 and R_2 is

$$N_A = \frac{1}{2(R_2-R_1)\left[\sigma_A(\lambda on)-\sigma_A(\lambda off)\right]} \ln\left[\frac{Pr_{on}(R_1)\ x\ Pr_{off}(R_2)}{Pr_{off}(R_1)\ x\ Pr_{on}(R_2)}\right] . \quad (28)$$

The quantities in equation 28 which are measured experimentally are the on and off wavelength returns at R_1 and R_2. Equation 28 can be rewritten as follows.

$$\frac{Pr_{on}(R_2)/Pr_{on}(R_1)}{Pr_{off}(R_2)/Pr_{off}(R_1)} = e^{\{-2(R_2-R_1)N_A[\sigma_A(\lambda on)-\sigma_A(\lambda off)]\}} \quad (29)$$

The term on the left is just the transmittance of the gas of interest in the range cell from R_1 to R_2. The exponent is the optical depth of the absorbing gas in the range cell. So from the error in determining the transmittance, which is the experimentally measured quantity, the corresponding error in determining the optical depth can be determined, and, assuming that the absorption cross section is known, the error in determining the concentration.

The procedure then will be to select appropriate on and off wavelengths using available SO_2 spectra in the .4 μm and 300 nm wavelength regions. The absorption cross sections for the on and off wavelength will be used to make a plot of error in optical depth or absorber concentration as a function of optical depth or absorber thickness for a given error in measuring the transmittance where the absorber thickness is $2(R_2-R_1)N_A$.

The spectrum of the $\nu_1+\nu_3$ combination band of SO_2 near 4 μm has been studied by a number of workers[2,3,4] using grating spectrometers with resolutions ranging from .017 cm^{-1}[4] to .48 cm^{-1}[2]. Recently, Pine[5] has studied the $\nu_1+\nu_3$ band using a cw difference-frequency spectrometer with a resolution

of .0003 cm^{-1}. Figure 2 shows an absorption coefficient spectrum, observed by Pine[5], under atmospheric conditions. Using figure 2, a line pair of 2498.5 cm^{-1} and 2500.8 cm^{-1} was chosen for analysis, with the on wavelength line having a frequency of 2498.5 cm^{-1} and the off wavelength line having a frequency of 2500.8 cm^{-1}. The on wavelength absorption cross section is .5 $(m\% \text{ atm})^{-1}$ and the off wavelength absorption cross section is 0 within Pine's error of $\pm$ .02 $(m\% \text{ atm})^{-1}$.

The spectrum of SO_2 near 300 nm was measured by Thompson[6] with a resolution of .02 nm. Figure 3 shows an absorption coefficient spectrum observed by Thompson[6]. Using figure 3, a line pair of 299.4 nm and 300.0 nm was chosen. The on wavelength, 300.0 nm, has an absorption cross section of 33.1 $(\text{atm-cm})^{-1}$. The off wavelength, 299.4 nm, has an absorption cross section of 7.28 $(\text{atm-cm})^{-1}$. The differential absorption cross section $\left[\sigma_A(\lambda_{on}) - \sigma_A(\lambda_{off})\right]$ is then 25.8 $(\text{atm-cm})^{-1}$.

Figure 4 shows error in optical depth or absorber concentration as a function of optical depth for errors in measuring the transmittance of 1, 2, 5, and 10 percent. Also shown on the abscissa are the absorber thicknesses corresponding to the 4 μm differential absorption, the 300 nm differential absorption, and the 299.4 nm off line absorption.

Note that for any given error in measuring the transmittance, the minimum error in the concentration determined from that measurement occurs for that combination of concentration and range cell for which the optical depth is equal to 1. Also the minimum error in determined concentration is approximately three times the error in measuring the transmittance.

Assuming a range cell of 100 meters and a 5% error in measuring the transmittance, at 4 μm the minimum detectable average concentration in the range cell is about 5½ parts per million and apparently the maximum detectable concentration is approximately 300 parts per million. The upper limit is actually much higher since the on wavelength could be tuned to a point where the absorption coefficient and therefore the optical depth are lower.

At 300 nm, again assuming a 100-meter range cell and 5% error in measuring transmittance, the minimum detectable concentration is about 110 parts per billion. The maximum detectable concentration is determined by the point where the absorption of the off wavelength line is so great that the return from the far side of the range cell cannot be measured accurately. For a 100-meter range cell and 5% error in measuring transmittance, the maximum detectable concentration is 20 ppm. Thus, for measurements of powerplant emissions, the DIAL instruments operating at 300 nm and 4 μm are complementary.

Assuming 5% error in measuring transmittance, a one kilometer column content measurement of SO_2 concentration as low as 11 parts per billion could be made using the DIAL technique at 300 nm.

It should be emphasized that this analysis has not considered what accuracy in measuring transmittance is achievable. For any specific system, this would have to be determined from a consideration of specific system parameters such as that made by Thompson[7].

Experimental Support for NASA Langley Plume Dispersion Program

In the early part of 1976 an agreement was made by NASA Langley Research Center and the Maryland Power Plant Siting Program to perform a joint experiment to determine the utility of the lidar as a method for characterizing plume rise and plume dispersion from power plants. In support of that experiment, a mobile lidar system was built using NASA equipment by personnel from Old Dominion University, NASA, and Wyle Laboratories.

Operation of the system was checked during late July by observing the plume from the VEPCO plant at Yorktown, Virginia.

In this report, the lidar system will be described. A later report will describe the design of the joint field experiment and the results of that experiment.

The lidar system consists of a ruby laser, a telescope receiver, a detector package, and associated instrumentation. The laser, telescope, and detector package are mounted on a searchlight-type mount with tracking capability. The entire system, including instrumentation and the searchlight mount, is contained on a flat-bed trailer.

The laser used in the system is a Holobeam 600 Q-switched ruby laser with a beam divergence of 3½ milliradians. The beam divergence was reduced to approximately 1 milliradian by using an up-collimating telescope at the output of the laser. The output energy of the laser can

vary from .75 to 2.0 joules with a pulse length of 30 nanoseconds. Thus, the ultimate range resolution attainable with the system is 4.5 meters.

The receiver is a 12-inch Cassegrain type telescope with a field of view of approximately 4 milliradians. The detector package has provision for mounting two photomultiplier tubes for extended dynamic range. For the plume dispersion experiment, only one tube was used. An RCA 7265 photomultiplier tube was selected for use in the system since it was sensitive to the 694 nanometer laser radiation, and it could be easily gated to prevent overload from the close-in return.

The instrumentation used consists of a high voltage power supply and gating circuit for the photomultiplier tube, pulse generators used for timing, and the data acquisition system.

The data acquisition system is based on a Digital Equipment Corporation model PDP11/10 minicomputer. The lidar return signal from the photomultiplier is recorded by a Biomation 8100 transient digitizer which can record 2000 8-bit words of data at sample rates up to 100 MH_z. The Biomation has an analog output so that the data can be displayed continuously on an oscilloscope and a digital output from which the computer accepts the recorded data. Other data accepted by the computer include laser energy,

laser shot counter reading, and elevation and azimuth angle from the searchlight mount. The data from each laser firing is immediately recorded on magnetic tape for later processing using either the PDP 11/10 or the main Langley Research Center computer facility. Also attached to the minicomputer is a Ramtek Graphics display which can display information in 16 shades of gray on an ordinary black and white television monitor.

The computer has been programmed to allow data processing to proceed simultaneously with data recording. This permits preliminary data analysis (such as range correction), and display on a nearby real-time basis. Three different types of data display are available. One is called an A-scope display and is simply an x-y display with no intensity modulation of the display. Another type of display, called a z-scope display, is useful for applications where the lidar is pointed vertically. This display plots intensity versus height on a vertical line using the 16-shade gray scale modulation. The third type of display is the RHI or range, height, intensity display which is used for displaying plume dispersion lidar returns. For this display, the horizontal axis corresponds to the horizontal distance from the lidar and the vertical axis corresponds to height above the lidar. Intensity is then plotted along a line which corresponds to the lidar elevation angle.

The lidar was tested during late July by observing the plume from the VEPCO plant at Yorktown. The plant is oil fired with no precipitators on the exhaust. The stack is 550 feet high. The lidar was located approximately 5.5 km from the stack with a viewing window about 30^{o} to either side. The plume was easily observable at a range of 8 km from the lidar and at a distance of 4 km downwind from the plant. Because of the restricted viewing window, the maximum useful range of the lidar could not be determined, but it is certainly greater than 8 km.

During the test, malfunctions in some of the computer peripherals occurred and shortcomings in the software were found. These problems were all corrected before the joint experiment in Maryland.

B. Work Done by ODU Resident Faculty.

ODU faculty devoted themselves to three main support efforts. First, Dr. Kindle and Dr. Blais consulted with Langley personnel on feasibility of field test procedures. Second, information was assembled on local climatology and on stack parameters of local sources for support of the Yorktown plume field test. Third, Dr. Blais initiated development of an adaptation to the Gaussian plume model using a surface interaction parameter first suggested by Csanady*. Geometric characteristics capable of lidar detection were proposed. Work is continuing on an error and sensitivity analysis of the modified model to make it more suitable for field application. Dr. Blais' report constitutes the appendix.

---

*G. T. Csanady, Aust. J. Phys. 8, 545-550 (1955).
G. T. Csanady, Aust. J. Phys. 10, 559-564 (1957).

END NOTES

1. S. K. Poultney, M. L. Brumfield, and J. H. Siviter, "A Theoretical Experimental Program to Develop Active Optical Pollution Sensors: Quantitative Remote Raman Lidar Measurements of Pollutants from Stationary Sources." NASA TMX-72887 (also Old Dominion University Research Foundation Technical Report PGSTR-PH75-12).

2. R. D. Shelton, A. H. Nielson, and W. H. Fletcher, J. Chem. Phys. 21, 2178 (1953).

3. R. J. Corice, K. Fox, and G. D. T. Tejwani, J. Chem. Phys. 59, 672 (1973). (Also Report No. UTPA-ERAL-03, Dept. of Phys. and Astron., U. of Tenn.)

4. A. Barbe, C. Secroun, P. Jouve, B. Duterage, N. Monnanteuil, J. Bellet, and G. Steenbeckeliers, J. Mol. Spectrosc. 55, 319 (1975).

5. A. Mooradian and A. S. Pine, "Tunable Laser Spectral Survey of Molecular Air Pollutants," NSF/RANN/AEN 71-01922 A02, M.I.T. Lincoln Laboratory (May 1976).

6. R. T. Thompson, Jr., J. M. Hoell, Jr., and W. R. Wade, Jour. of Applied Physics 46, 3040 (1975).

7. R. T. Thompson, Jr., "Differential Absorption and Scattering Sensitivity Predictions," NASA CR-2627. (Also Old Dominion University Research Foundation Technical Report PGSTR-PH75-19.)

Figure 1. Laser line shapes.

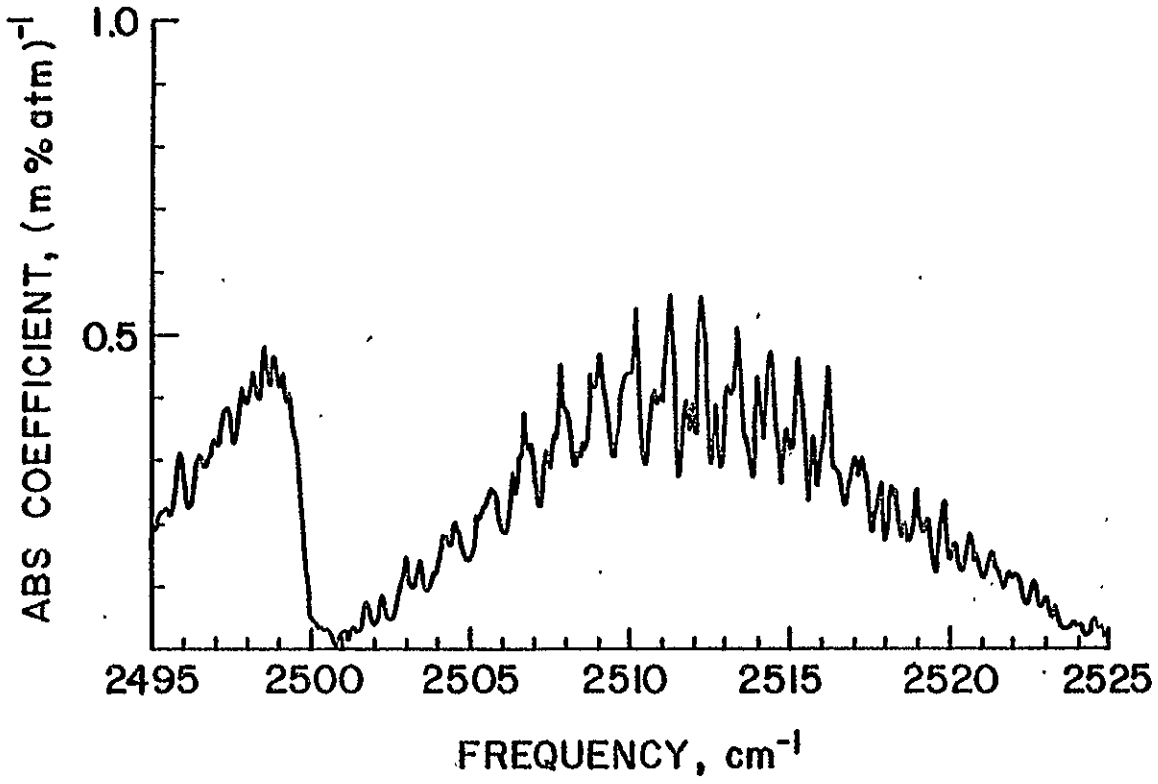

Figure 2. Absorption spectrum of the $\nu_1 + {}_3$ band of SO_2 at atmospheric pressure (after Pine[5]).

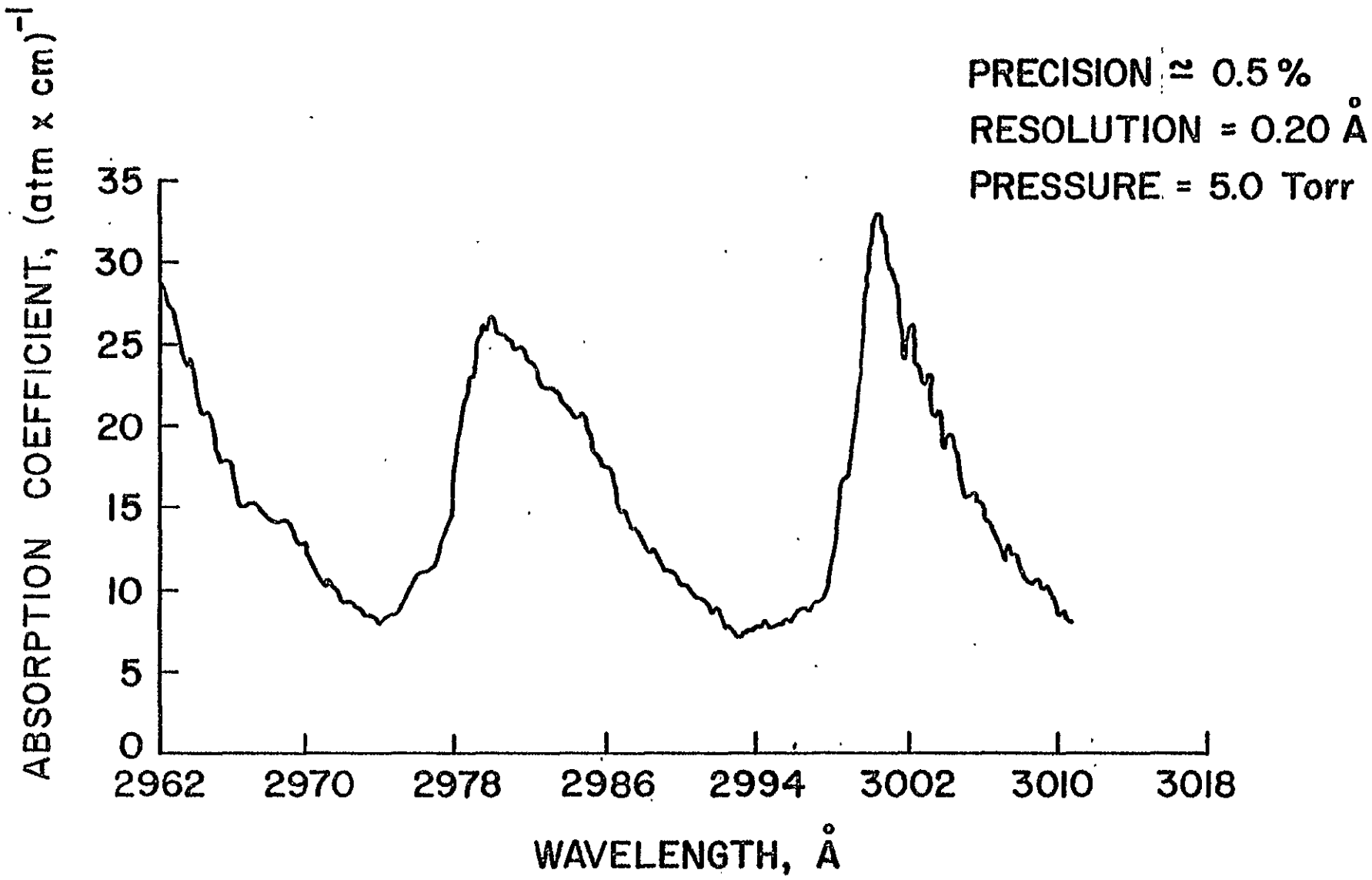

Figure 3. Absorption spectrum of SO_2 near 300 nm (after Thompson[6]).

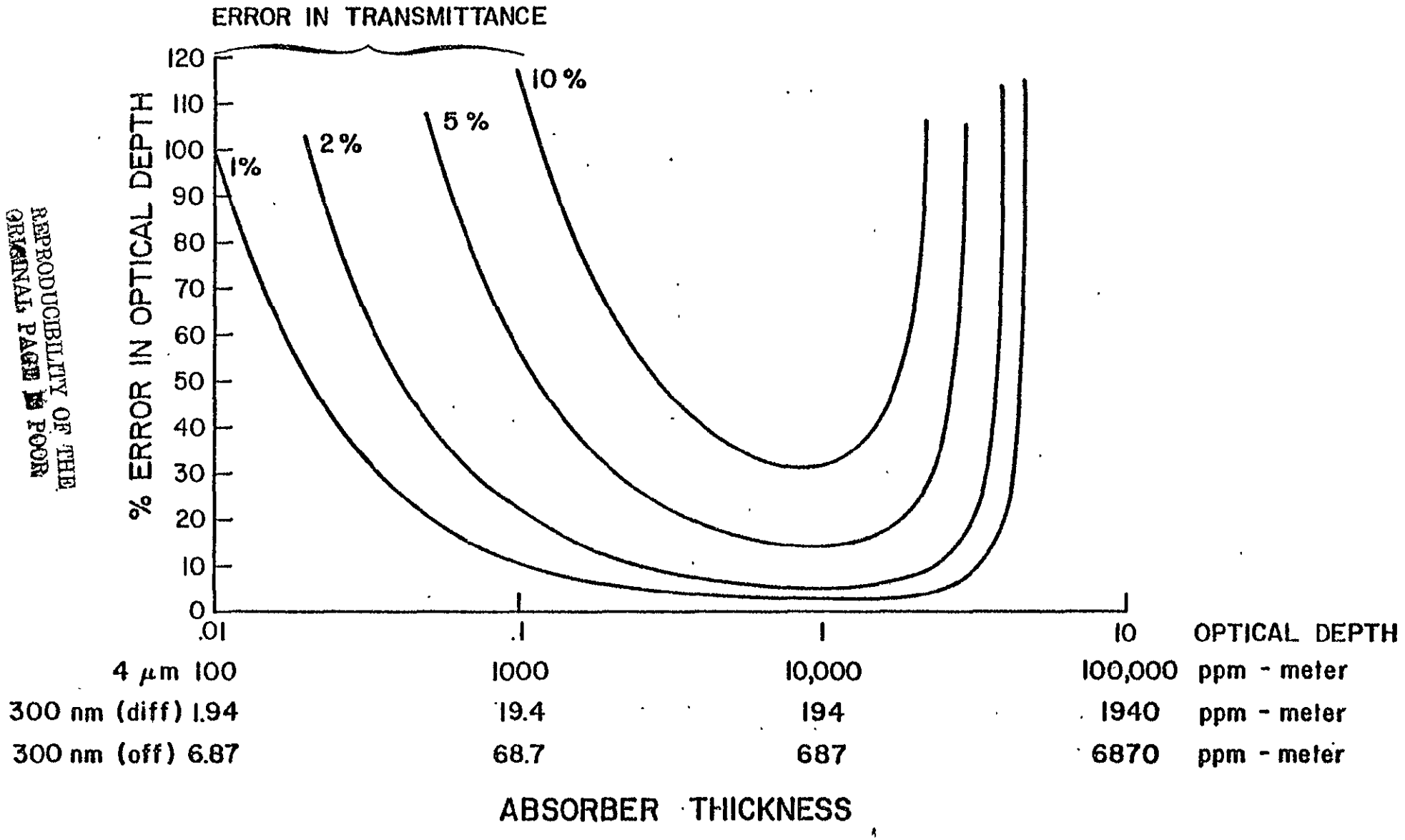

Figure 4. Error in optical depth or absorber concentration as a function of optical depth or absorber thickness for various errors in measuring transmittance.

APPENDIX

LIDAR DETECTABLE GEOMETRIC CHARACTERISTICS OF GAUSSIAN PLUME MODELS WITH VARIABLE SURFACE BOUNCE

Roger N. Blais

Department of Physics and Geophysical Sciences

Old Dominion University

Norfolk, Virginia 23508, U.S.A.

Abstract - A Gaussian Plume Model is proposed containing a dimensionless bounce parameter, β, the fraction of material dispersed to the earth's surface that is reflected into the plume. The $\beta = 0$ case yields the free space plume in the $z > 0$ domain, with perfect trapping of effluent on the $z = 0$ plane. The $\beta = 1$ case reproduces the Pasquill-Gifford Model with all effluent reflected at the surface. The model is formulated to allow estimation of β from lidar measurements of plumes over various textures of flat terrain (e.g. forest, grass). Lidar detectable geometric characteristics of plumes are described as functions of a non-dimensional downwind distance parameter, σ_z/H, and of β as it ranges from 0 to 1. These characteristics are the altitude of maximum concentration, and the mean altitude of the concentration. The measured mean altitude's dependence on the maximum altitude of lidar sampling is discussed. The influence of β on the total downwind flux of effluent and on surface concentration is described.

NOMENCLATURE

$C(x,y,z)$	concentration of effluent, kg m^{-3}
H	effective emission height, the sum of stack height and plume rise, m
$M_n(\mu)$	n^{th} moment of η integrated over Λ_0 from $\eta = 0$ to $\eta = \mu$, see Equation 8, dimensionless
Q	rate of effluent emission at source (0,0,H), kg s^{-1}
Q_i	rate of effluent emission by virtual image source at (0,0,-H), kg s^{-1}
U	mean wind speed, m s^{-1}
x,y,z	downwind, crosswind and vertical coordinates respectively, m
α	normalized vertical plume thickness, dimensionless
β	the dimensionless surface bounce parameter such that $0 \leq \beta \leq 1$.
η	normalized altitude, dimensionless
η_m	η at which maximum Λ_0 occurs, dimensionless
$\bar{\eta}_\mu$	mean (expectation) value of η averaged over Λ_0 from $\eta = 0$ to $\eta = \mu$
$\Lambda(\alpha,y,\eta)$	normalized concentration of effluent, see Equation 4, dimensionless
$\Lambda_0(\alpha,\eta)$	normalized concentration of effluent on $y = 0$ plane, see Equation 5, dimensionless
μ	the maximum normalized altitude to which lidar measurements are made, dimensionless
$\sigma_y(x)$	standard deviation of $C(x,y,z)$ relative to y, m
$\sigma_z(x)$	standard deviation of $C(x,y,z)$ relative to z in free space, m
$\Phi(\alpha,\beta)$	total normalized mass flux through a vertical plane normal to the wind, see Equation 16, dimensionless

LIST OF CAPTIONS

Fig. 1. η_m, the altitude of maximum A_0, as a function of normalized downwind distance parameter, α.

Fig. 2. Altitude of the true mean ($\bar{\eta}_\infty$), of a measured mean with sampling interval $0 \leq \eta \leq 3$ ($\bar{\eta}_3$), and the altitude of maximum normalized concentration (η_m).

Fig. 3. The normalized flux ($\Phi(\alpha)$) or fraction of original effluent mass still airborne at α, and the $\bar{r}_\infty$ normalization factor ($M_0(\infty)$).

INTRODUCTION

The growing use of the Gaussian Plume Model (Csanady, 1973; Seinfeld, 1975; Sutton, 1932; Turner, 1970) for the design of stacks, for the preparation of environmental impact statements, and for the development of multiple source models (TRW, 1969) makes the validity of the assumptions upon which the model rests a legitimate economic and public health concern. Chamberlain (1966), Bessemoulin (1974), Heines (1974), Ragland (1975), and Seguin (1973), among others, have examined the boundary conditions at the earth's surface. The influence of the surface on the plume is amenable to lidar (laser radar) study if a simple field model can be used to relate vertical concentration profiles to a parameter that describes the surface. Lidar is better able to establish plume geometric characteristics than to define absolute mass concentrations, due to the difficulties of the Mie scattering problem for polydisperse aerosols. Field workers are seldom able to measure all the necessary input variables, which include the complex index of refraction for each of the various constituents, and their particle size and shape distributions (Diermendjian, 1969). Geometric characteristics of a plume, however, are readily defined under simple assumptions of particle homogeneity and isotropy in the spatial domain.

In addition, lidar systems can time average data over periods consistent with the assumptions of the Gaussian Models. In this regard, lidar is superior to instantaneous photogrammetric techniques (Blais, 1975).

This paper considers lidar detectable plume geometric characteristics capable of illuminating surface interactions, by exploiting a simple generalization of the Pasquill-Gifford Model (Gifford, 1961; Hay, 1957; Pasquill, 1961). As in the standard model, the surface is required to be relatively flat, but its texture may vary widely in effective porosity. The generalization is based on a surface bounce parameter. Non-dimensional expressions for altitude of maximum concentration, for true and for measured mean altitude of concentration, and for downwind flux are presented as functions of a non-dimensional downwind distance parameter, and of the surface bounce parameter. The influence of β on surface level concentrations is discussed.

THE BASIC MODEL

The Pasquill-Gifford Model is modified by including a dimensionless bounce parameter, β, which ranges between zero and one. It multiplies the surface reflectance term such that:

$$C = \left(\frac{Q}{2\pi U\sigma_y\sigma_z}\right)\exp\left(-\frac{y^2}{2\sigma_y^2}\right)\left[\exp\left(-\frac{[z-H]^2}{2\sigma_z^2}\right) + \beta\exp\left(-\frac{[z+H]^2}{2\sigma_z^2}\right)\right] \quad (1)$$

In the case $\beta = 1$, presumed to be typical of a smooth flat surface, all of the material dispersed downward to the earth's surface remains airborne because it is bounced or reflected back into the plume. This is the condition for the regular Pasquill-Gifford model. The opposite extreme case, $\beta = 0$, presumed to be approximated by dense forest, implies total absorption of material at the earth's surface. The plume then behaves as a free space plume in the domain $z > 0$.

The β parameter arises from the artifice of using a virtual image source located at $x = y = 0$, $z = -H$ to account for reflectance at the earth's surface. Usually, the rate of image source emission, Q_i, is assumed to be equal to the real source emission rate, Q. Because the surface concentration depends upon summing the effects of the real and the image source, and because $Q_i > Q$ is not physically meaningful, the $Q_i = Q$ case represents the highest possible surface concentration at any given field point. This worst case is useful in predicting the environmental impact of

proposed smokestacks. The true influence of the surface on plume material is undoubtedly between the extremes represented by $\beta = 1$ and $\beta = 0$, where, mathematically β is defined as:

$$\beta \equiv Q_i/Q, \qquad (2)$$

though physically it is dependent on surface properties.

The presumed illustrative examples of smooth flat land implying $\beta \simeq 1$, and of dense forest implying $\beta \simeq 0$, bear further comment. For a single value of β to characterize plume dispersal requires that the terrain is flat, and uniform, and that the plume is not influenced by complicating factors like penetration of the inversion, or trapping by the top of the mixing layer. Given such conditions, two surfaces may be compared, both of which are flat and smooth, but which differ in porosity. The first surface is exemplified by a smooth hard surface, like pavement, or closely mowed grass. The second surface is dense forest canopy. The forest has a stagnant air layer beneath the canopy, and a comparativel enlarged ratio of absorbing surface area to land surface area. Thus, it is anticipated that forest will be a poorer reflector, and a better absorber of effluent than pavement, or mowed grass. Consequently, one expects $\beta_{forest} < \beta_{pavement}$. Lidar studies can determine values for β over diverse, but uncomplicated, surfaces like water, swamp or moorland.

THE NORMALIZED MODEL

It is useful to formulate the model non-dimensionally, so that it is independent of particular functional forms of $\sigma_y(x)$ or $\sigma_z(x)$. The following dimensionless quantities are defined.

$$\alpha \equiv \frac{\sigma_z}{H}, \qquad \eta \equiv \frac{z}{H}, \quad \Lambda \equiv \frac{2\pi U \sigma_y C H}{Q}. \qquad (3)$$

Note that σ_z generally increases with x (Turner, 1970) and H is constant in the region of interest far enough downwind for surface bounce to be significant. Consequently, α is a measure of x, in that $\alpha \to 0$ as $x \to 0$, and $\alpha \to \infty$ monotonically as $x \to \infty$. The relationship is non-linear, however, and depends upon stability class.

Note also that Λ is slightly different from the usual normalized concentration parameter, CU/Q, which is dimensionally a reciprocal area. As will be seen, Λ is more convenient in the present formulation, because it absorbs the σ_y dependence of the model.

Substituting Equations 3 into Equation 1, and isolating β by the extraction of a common monomial factor yields

$$\Lambda(\alpha,y,\eta) = \alpha^{-1}\exp\left(-\frac{y^2}{2\sigma_y^2} - \frac{[\eta+1]^2}{2\alpha^2}\right)\left[\exp\left(\frac{2\eta}{\alpha^2}\right) + \beta\right]. \qquad (4)$$

Next, defining $\Lambda_0(\alpha,\eta) \equiv \Lambda(\alpha,0,\eta)$ yields

$$\Lambda_0(\alpha,\eta) = \alpha^{-1}\exp\left(-\frac{[\eta+1]^2}{2\alpha^2}\right)\left[\exp\left(\frac{2\eta}{\alpha^2}\right) + \beta\right]. \qquad (5)$$

Thus, Λ_0 represents the non-dimensional concentration on the plume vertical plane of symmetry. There are three reasons

for dealing with Λ_0 rather than with Λ. First, a lidar system samples along an entire line of sight. In the downwind region where the plume is sufficiently tenuous for multiple optical scattering events to be insignificant, but for surface bounce to be influential, one can find the centroid of the plume and plot vertical profiles through that plane only. Next, even if one wishes to examine the total optical brightness of the plume due to diffuse scattered light, an integration of total mass load, Λ, along an infinite horizontal cross-wind line of sight (from $y = -\infty$ to $y = +\infty$) would differ from Λ_0 only by the multiplicative factor $\sqrt{2\pi}\,\sigma_y$. Finally, some regional multiple source models, like the AQDM (TRW, 1969), use a Gaussian vertical dependence, consistent with Λ_0, but a non-Gaussian horizontal dependence incompatible with Λ.

GEOMETRIC PROPERTIES OF Λ_0

To use the above model for estimating β, the lidar system in the field must acquire the following data. Profiles of Λ_0 versus η are determined at a given value of α. To accomplish this, the lidar must aim in a horizontal cross-wind direction, and scan vertically between $\eta = 0$ and a maximum normalized altitude $\eta = \mu$. Acquired data must be stored and the lidar then changes azimuth to make a second Λ_0 versus η profile at a new α. After measuring profiles for several α values, the entire sequence is repeated, until time averaged profiles are established for each α. Averaging times should be commensurate with the assumptions underlying the Gaussian Model (Slade, 1968). Two physical properties of the profiles are then established: η_m, the altitude of maximum Λ_0; and $\bar{\eta}_\mu$, the mean altitude or expectation value of η over the $\Lambda_0(\alpha,\eta)$ distribution measured from $\eta = 0$ to $\eta = \mu$.

Altitude of Maximum Concentration.

The normalized altitude of maximum Λ_0 is derived by maximizing Equation 5 with respect to η. The resulting equation is transcendental, with no explicit expression for η_m as a function of α and β. It can be written in the following form:

$$\beta = \left(\frac{1-\eta_m}{1+\eta_m}\right) \exp\left(\frac{2\eta_m}{\alpha^2}\right). \qquad (6)$$

Values of η_m that satisfy Equation 6 are plotted for various values of β in Fig. 1. As expected, near the source ($\alpha \to 0$) surface bounce does not influence η_m, which approaches one regardless of β. This is to say Λ_0 is a maximum at $z = H$. In the downwind direction β does strongly influence the altitude of maximum concentration. As $\alpha \to \infty$, $\eta_m \to (1-\beta)/(1+\beta)$ asymptotically. As a result, the $\beta = 0$ case, with no surface bounce, leaves $\eta_m = 1$ for all α. For $\beta = 1$ or complete surface bounce, $\eta_m \to 0$, which is to say the peak value descends to the earth's surface, a fact recently pointed out by Dumbauld (1976). Yet, η_m only descends to the $\eta = 0$ plane if $\beta \equiv 1$, and in that case $\eta_m = 0$ for all $\alpha \geq 1$. Finally, one notes η_m is a strong function of β for $\alpha \geq 1$, allowing it to serve as a primary detection characteristic of β according to Equation 6.

In application, H is estimated from standard plume rise formulas (Briggs, 1969), and the altitude, z, of maximum Λ_0 is measured from the lidar vertical scans. Dividing z by H yields η_m. Next, σ_z is estimated from the stability class and downwind distance x, using the graph on page 9 of Turner (1970). Then α is computed from Equation 3. Equation 6 is used to compute β from η_m and α. A value of β is calculated for each α, and if the surface is simple, one expects them to be approximately equal. A least squares method can be used to estimate β for the surface, provided the values are not excessively scattered. Measurements under various stability

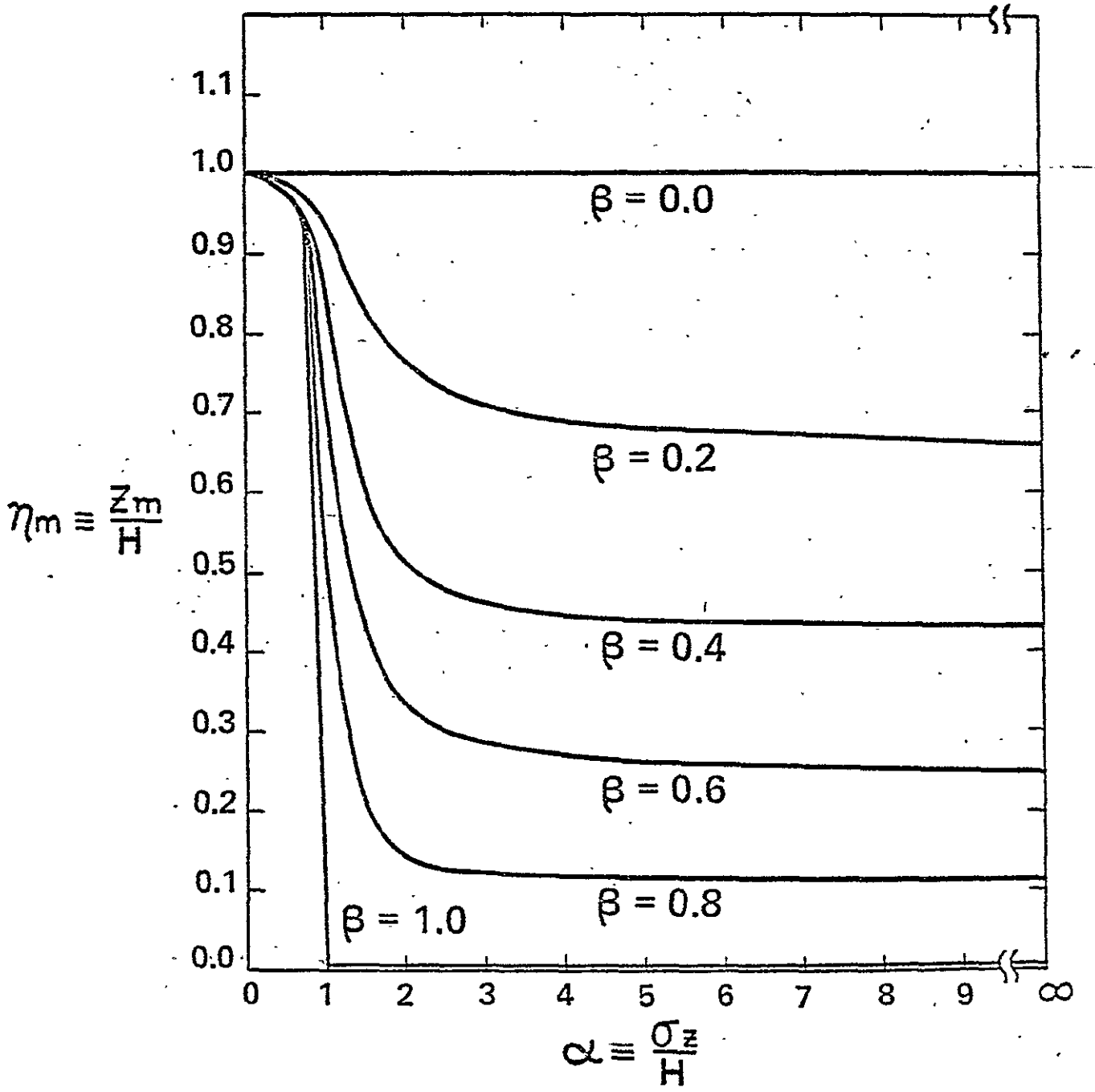

Fig. 1. η_m, the altitude of maximum Λ_0, as a function of normalized downwind distance parameter, α.

conditions can examine the repeatability of β for a given surface.

Mean Altitude of Concentration. A second method of determining β is less sensitive and involves more computation than the above method, but it does offer an independent check on the model's internal consistency. The second method is to measure the mean altitude (expectation value of the altitude) using the normalized concentrations, Λ_0, as a distribution function that weights η. The mean altitude, $\bar{\eta}_\mu$, depends upon the sampling interval (from η = 0 to η = μ) and is defined as:

$$\bar{\eta}_\mu = \frac{M_1(\mu)}{M_0(\mu)} \qquad (7)$$

where $M_n(\mu)$ is the n^{th} moment of η with respect to Λ_0, defined by

$$M_n(\mu) \equiv \int_0^\mu \eta^n \Lambda_0 d\eta \qquad (8)$$

Performing the integration indicated by Equation 8 with n = 0 and n = 1 gives the zeroeth and first order moments,

$$M_0(\mu) = \sqrt{\frac{\pi}{2}}\left[(1-\beta)\,\mathrm{erf}\left(\frac{1}{\sqrt{2}\alpha}\right) + \mathrm{erf}\left(\frac{\mu-1}{\sqrt{2}\alpha}\right) + \beta\,\mathrm{erf}\left(\frac{\mu+1}{\sqrt{2}\alpha}\right)\right], \qquad (9)$$

and

$$M_1(\mu) = \sqrt{\frac{\pi}{2}}\left[(1+\beta)\,\mathrm{erf}\left(\frac{1}{\sqrt{2}\alpha}\right) + \mathrm{erf}\left(\frac{\mu-1}{\sqrt{2}\alpha}\right) - \beta\,\mathrm{erf}\left(\frac{\mu+1}{\sqrt{2}\alpha}\right)\right]$$

$$+\alpha\left[(1+\beta)\exp\left(-\frac{1}{2\alpha^2}\right) - \exp\left(-\frac{[\mu-1]^2}{2\alpha^2}\right) - \beta\exp\left(-\frac{[\mu+1]^2}{2\alpha^2}\right)\right], \qquad (10)$$

where erf(t) is the normal error function, defined

$$\mathrm{erf}(t) \equiv \frac{2}{\sqrt{\pi}} \int_0^t \exp(-u^2)\,du. \qquad (11)$$

Dividing Equation 10 by Equation 9 yields $\bar{\eta}_\mu$, as shown by Equation 7. The expression for $\bar{\eta}_\mu$ is rather formidable, but several limiting expressions derived from Equation 9 and 10 make it more comprehensible. See Fig. 2.

First, it is to be expected that near the source ($\alpha = 0$) bounce plays an insignificant role, so that $\bar{\eta}_\mu$ is independent of β, and furthermore, that $\bar{\eta}_\mu = 1$ at $\alpha = 0$. That is to say, the mean altitude of effluent at $x = 0$ is $\eta = 1$ or $z = H$. By noting that

$$\lim_{t\to\infty} \mathrm{erf}(t) = 1 \qquad (12)$$

and taking the limit of $M_0(\mu)$ and $M_1(\mu)$ as $\alpha \to 0$ one discovers

$$\lim_{\alpha\to 0} M_0(\mu) = \sqrt{2\pi}\,, \qquad \lim_{\alpha\to 0} M_1(\mu) = \sqrt{2\pi} \qquad (13)$$

Thus, as expected, their ratio, $\bar{\eta}_\mu = 1$ at the source. In Fig. 2 all values of $\bar{\eta}_\mu$ (and η_m) approach 1 as α approaches 0.

Next, the behavior of the expression M_0 and M_1 are simplified if μ is allowed to approach infinity. Physically, this corresponds to the case of sampling the plume over an unlimited range of altitude from $\eta = 0$ to $\eta = \infty$. In that case, the quantity $\bar{\eta}_\infty$ may be called the "true" mean altitude of the plume. The values of M_0 and M_1 become

$$\lim_{\mu\to\infty} M_0(\mu) \equiv M_0(\infty) = \sqrt{\frac{\pi}{2}}\left[(1-\beta)\,\mathrm{erf}\left(\frac{1}{\sqrt{2\alpha}}\right) + (1+\beta)\right] \qquad (14)$$

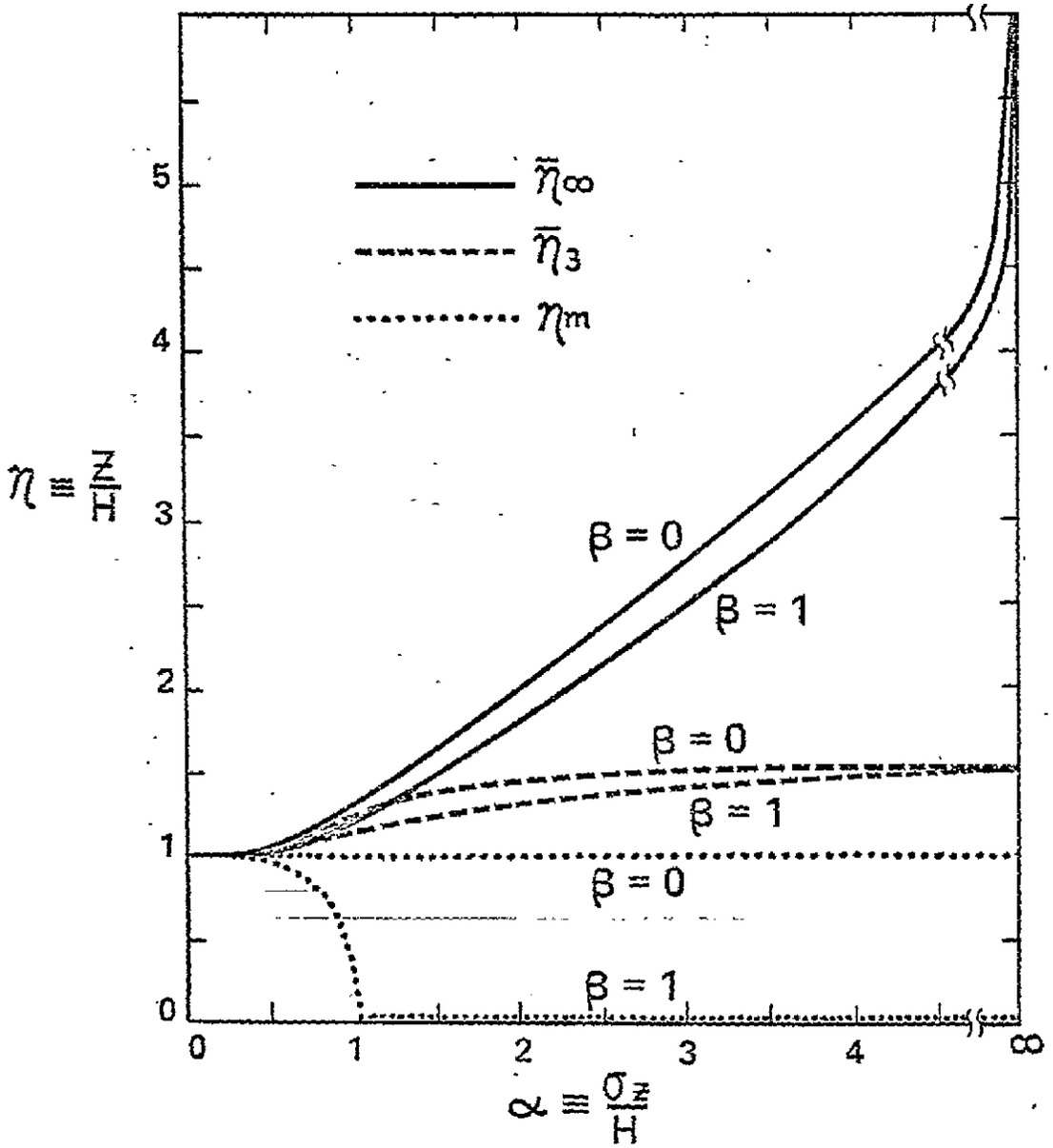

Fig. 2. Altitude of the true mean ($\bar{\eta}_\infty$), of a measured mean with sampling interval $0 \leq \eta \leq 3$ ($\bar{\eta}_3$), and the altitude of maximum normalized concentration (η_m).

and

$$\lim_{\mu\to\infty} M_1(\mu) \equiv M_1(\infty) = \sqrt{\frac{\pi}{2}}\left[(1+\beta)\,\mathrm{erf}\left(\frac{1}{\sqrt{2}\alpha}\right) + (1-\beta)\right]$$

$$+ \alpha(1+\beta)\exp\left(-\frac{1}{2\alpha^2}\right). \qquad (15)$$

Their ratio, $\bar{\eta}_\infty$, is plotted in Fig. 2 as the top pair of lines for the two cases $\beta = 0$ and $\beta = 1$. One sees that $\bar{\eta}_\infty$ expands without bound as $\alpha \to \infty$ far downwind from the source. This occurs because Equation 14, the denominator of Equation 7, remains finite as α increases, but Equation 15, the numerator, has a final term that increases without limit as α does likewise. Thus, the true mean altitude of the normalized concentration rises above H the farther downwind the plume travels.

Having examined the behavior of $\bar{\eta}$ near the source ($\alpha = 0$), and for the case of infinite vertical sampling, it remains to consider the "measured" mean altitude of Λ_0, $\bar{\eta}_\mu$. This measured value is achieved by allowing the measured Λ_0 versus η profile to be truncated at an upper bound, $\eta = \mu$. True lidar systems will only scan to altitudes of η equal to a small number. Because all values of η larger than μ are considered to contribute nothing to the computation of $\bar{\eta}_\mu$, clearly $\bar{\eta}_\mu < \bar{\eta}_\infty$ for all finite μ. Use of Equations 7, 9, and 10 yields $\bar{\eta}_\mu$. A specific typical case, $\mu = 3$, is plotted as the middle pair of lines in Fig. 2, illustrating the two cases $\beta = 1$ and $\beta = 0$. (The bottom pair of lines in Fig. 2

merely repeat for comparison the $\beta = 0$ and $\beta = 1$ cases of η_m previously plotted in Fig. 1).

Note that $\bar{\eta}_\mu$ does not approach infinity as α increases, but instead remains finite throughout the entire range of α. Since only samples between $\eta = 0$ and $\eta = \mu$ are considered, the value of $\bar{\eta}_\mu$ must lie in the range $0 \leq \bar{\eta}_\mu \leq \mu$. Thus $\bar{\eta}_\mu$ is always finite.

Figure 2 reveals an additional noteworthy fact. The measured mean altitude, $\bar{\eta}_\mu$, is not nearly as strongly dependent upon β as η_m, the altitude of maximum A_0, is. Thus as stated above, the measured mean value is not as sensitive a measure of β as η_m is.

DOWNWIND FLUX

The Pasquill-Gifford Model has no built-in pollutant removal mechanism. Thus, mass flux at the source Q, is equal to the mass flux through any vertical, semi-infinite ($z > 0$) plane normal to the wind at any distance downwind from the source. If $\beta < 0$, however, some material is removed from the plume and therefore downwind flux is affected. Define a normalized flux, $\Phi(\alpha)$, a function of normalized downwind distance, α, as:

$$\Phi(\alpha) \equiv \frac{1}{2\pi\sigma_y} \int_0^\infty \int_{-\infty}^{\infty} \Lambda \, dy d\eta \quad . \tag{16}$$

Substitution from Equation 3 shows

$$\Phi(\alpha) = \int_0^\infty \int_{-\infty}^{\infty} \left(\frac{CU}{Q}\right) dy dz \tag{17}$$

where C is a function of α implicitly. Returning to Equation 16, and performing the y integration reveals

$$\Phi(\alpha) = \frac{\sqrt{2\pi}\ \sigma_y}{2\pi\ \sigma_y} \int_0^\infty \Lambda_0 \, d\eta = \frac{M_0(\infty)}{\sqrt{2\pi}} \quad . \tag{18}$$

Since $M_0(\infty)$ is $\sqrt{2\pi}$ at $\alpha = 0$, $\Phi(\alpha) = 1$ at the source. But $M_0(\infty)$ is a function of β as well as α. Figure 3 reveals this dependence. $\Phi(\alpha)$ is plotted on the left ordinate, and it may be considered the fraction of material emitted at the source that is still airborne at α. The right ordinate plots $M_0(\infty) = \sqrt{2\pi}\ \Phi(\alpha)$. It is also useful in computing $\bar{\eta}_\infty$, for it is the normalizing factor.

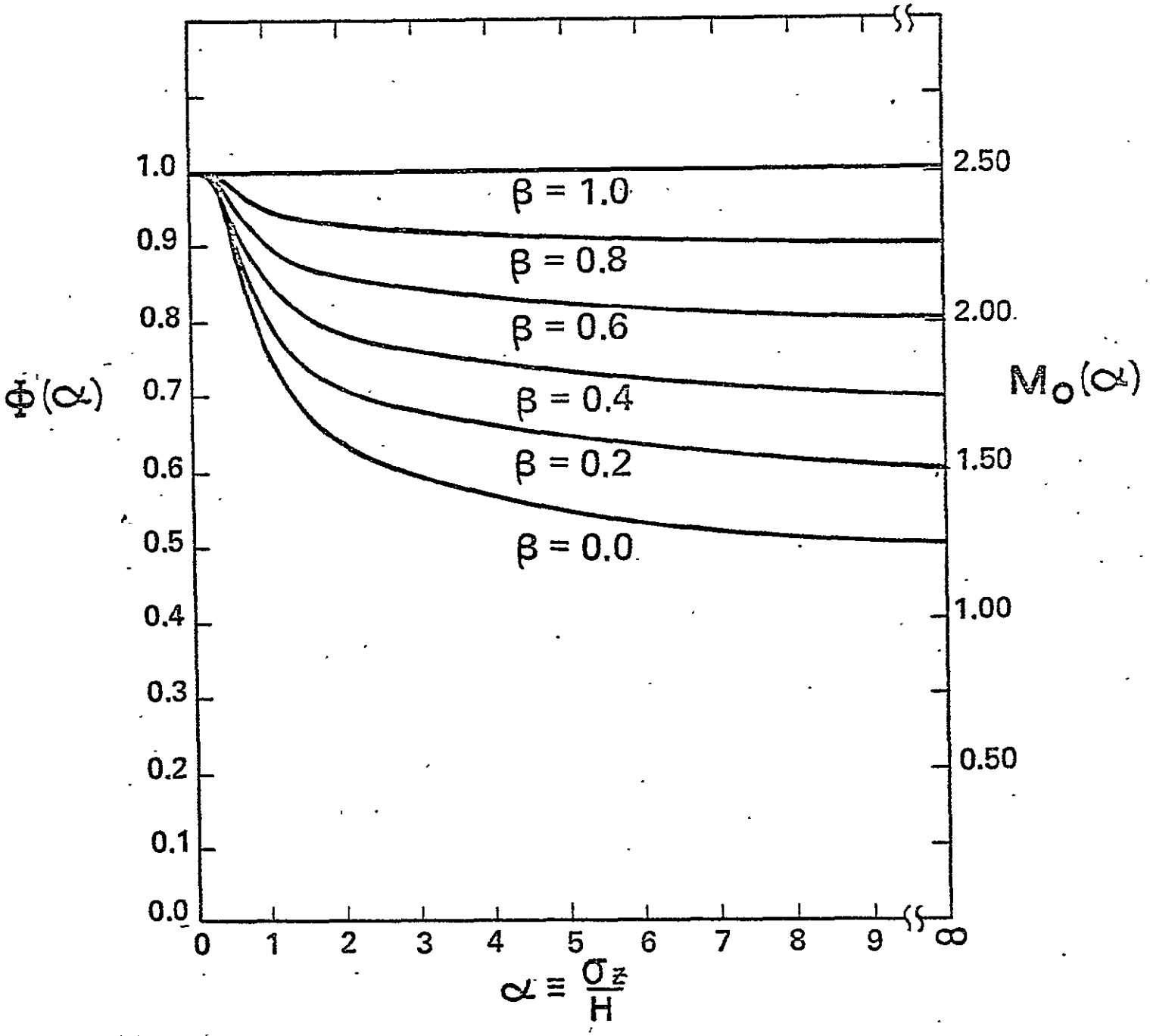

Fig. 3. The normalized flux ($\Phi(\alpha)$) or fraction of original effluent mass still airborne at α, and the $\bar{n}_\infty$ normalization factor ($M_0(\infty)$).

If $\beta = 0$ the matter dispersed downward from H is ultimately absorbed by the surface, but that borne upward remains aloft until other atmospheric processes invalidate the original assumptions of the model. Consequently, no more than half of the mass is ever removed from the plume by surface trapping.

INFLUENCE OF ε ON SURFACE CONCENTRATION

Since humans live on the earth's surface, it is worthwhile to investigate the significance of the ε value being less than one on surface concentrations. This is perhaps best seen in the more familiar basic model, rather than in the non-dimensional model. Thus, going back to Equation 1, and setting z = 0 yields

$$C = \frac{Q}{2\pi\sigma_y\sigma_z} \exp\left(-\frac{y^2}{2\sigma_y^2} - \frac{h^2}{2\sigma_z^2}\right)(1+\varepsilon) \qquad (19)$$

For the Pasquill-Gifford Model ε = 1. Then the final (1+ε) factor equals two. If the true value of ε is less than one, its influence on the surface concentration is clearly salutary but it only influences the concentration and not its geographic distribution.

CONCLUSION

In testing numerical models for plume dispersal with field experiments, it is common to reconcile discrepancies between predicted and measured values by adjusting source parameters. A simple adjustment in surface reflectance, β, would often accomplish the same reconciliation without disturbing source variables one has no reason to change without knowledge of vertical wind profiles and surface roughness. Future lidar experiments may find it profitable to study sources that disperse over a variety of simple, yet diverse terrains, such as forest, grassland and water in order to investigate the usefulness of a parameter β, and to see if it is itself independent of wind speed and stability class over a reasonable range of common conditions. If consistent values of β can be established, improvements in regional predictor models like the AQDM could be wrought.

ACKNOWLEDGEMENTS

The author wishes to thank E. C. Kindle and G. E. Copeland for helpful discussions, E. J. Blais for preparation of the graphs, and NASA Grant NSG-1060 for financial support.

REFERENCES

Bessemoulin P. and Benarie M. (1974) Contribution à l'étude de la diffusion des pollutants gazeux dans l'atmosphere. Atmospheric Environment 8, 261-279.

Blais R. N., Copeland G. E. and Lerner T. H. (1975) Use of LARS system for the quantitative determination of smoke plume lateral diffusion coefficients from ERTS images of Virginia. Remote Sensing of Earth Resources 4, University of Tennessee Space Institute, Tullahoma, Tennessee, 621-633.

Briggs G. A. (1969) Plume Rise, Publication No. TID-25075, NTIS, Springfield, Virginia 22151, U.S.A.

Chamberlain A. C. (1966) Transport of gases to and from grass and grass-like surfaces. Proc. Roy. Soc. London A290, 236-265.

Csanady G. T. (1973) Turbulent Diffusion in the Environment, pp. 208-217, Reidel, Dordrecht, Holland.

Deirmendjian D. (1969) Electromagnetic Scattering on Spherical Polydispersions. American Elsevier, New York.

Dumbauld R. K. and Bowers J. F. (1976) Point source atmospheric diffusion model - Discussion. Atmospheric Environment 10, 418.

Gifford F. A. (1961) Uses of routine meteorological observations for estimating atmospheric dispersion. Nuclear Safety 2, 4, 47-51.

Hay J. S. and Pasquill F. (1957) Diffusion from a fixed source at a height of a few hundred feet in the atmosphere. J. Fluid Mech. 2, 299-310.

Heines T. S. and Peters L. K. (1974) The effect of ground level absorption on the dispersion of pollutants in the atmosphere. Atmospheric Environment 8, 1143-1153.

Pasquill F. (1961) The estimation of the dispersion of wind-borne material. Meteorol. Mag. 90, 1063, 33-49.

Ragland K. W. (1975) Point source atmospheric diffusion model with variable wind and diffusivity profiles. Atmospheric Environment 9, 175-189.

Seguin B. (1973) Rugosité du paysage et diffusion atmospherique. Atmospheric Environment 7, 429-442.

Seinfeld J. H. (1975) Air Pollution: Physical and Chemical Fundamentals, pp. 272-280, McGraw-Hill, New York.

Slade D. H., ed. (1968) Meteorology and Atomic Energy, US AEC, Publication TID-24190, Oak Ridge, Tennessee

Sutton O. G. (1932) A theory of eddy diffusion in the atmosphere. Proc. Roy. Soc. London, A135, 143-165.

Turner D. B. (1970) Workbook of Atmospheric Dispersion Estimates. U. S. Environmental Protection Agency, AP-26.

TRW Systems Group (1969) Air Quality Display Model, Publication No. PB 189 194, p 2-4, NTIS, Springfield, Virginia 22151, U.S.A.

BEST SELLERS

FROM NATIONAL TECHNICAL INFORMATION SERVICE

Development of Pre-Mining and Reclamation Plan Rationale for Surface Coal Mines
PB-258 041/SET/ PAT 590 p. PC$22.50/MF$7.00

Manual of Respiratory Protection Against Airborne Radioactive Materials
PB-258 052/PAT 147 p. PC$6.00/MF$3.00

Design and Construction of a Residential Solar Heating and Cooling System
PB-237 042/ PAT 233 p. PC$8.00/MF$3.00

1976 Energy Fact Book
ADA-029 331/ PAT 195 p. PC$12.50/MF$12.50

Impacts of Construction Activities in Wetlands of the United States
PB-256 674/ PAT 426 p. PC$11.75/MF$3.00

Standardized Development of Computer Software. Part I: Methods
N76-30-849/ PAT 389 p. PC$10.75/MF$3.00

A Methodology for Producing Reliable Software, Volume I.
N76-29-945/ PAT 228 p. PC$8.00/MF$3.00

Flow and Gas Sampling Manual
PB-258 080/ PAT 102 p. PC$5.50/MF$3 00

Solar Heating and Cooling in Buildings: Methods of Economic Evaluation
COM-75-11070/ PAT 48 p. PC$4.00/MF$3.00

Data Base Directions. The Next Steps
PB-258 103/ PAT 177 p. PC$7.50/MF$3.00

Comparative Study of Various Text Editors and Formatting Systems
ADA-029 050/ PAT 93 p. PC Not Available/MF$3.00

Explaining Energy: A Manual of Non-Style for the Energy Outsider Who Wants In
LBL-4458/ PAT 78 p. PC$4.50/MF$3.00

A Survey of State Legislation Relating to Solar Energy
PB-258 235/ PAT 166 p. PC$6.75/MF$3.00

Cost Estimating Handbook for Transfer, Shredding and Sanitary Landfilling of Solid Waste
PB-256 444/ PAT 85 p. PC$5.00/MF$3.00

Coal Liquefaction Design Practices Manual
PB-257 541/ PAT 372 p. PC$10.50/MF$3.00

HOW TO ORDER

When you indicate the method of payment, please note if a purchase order is not accompanied by payment, you will be billed an additional $5.00 *ship and bill* charge. And please include the card expiration date when using American Express.

Normal delivery time takes three to five weeks. It is vital that you order by number or your order will be manually filled, insuring a delay. You can opt for *airmail delivery* for $2.00 North American continent; $3.00 outside North American continent charge per item. Just check the *Airmail Service* box. If you're really pressed for time, call the NTIS Rush Handling Service (703) 557-4700. For a $10.00 charge per item, your order will be airmailed within 48 hours. Or, you can pick up your order in the Washington Information Center & Bookstore or at our Springfield Operations Center within 24 hours for a $6.00 per item charge.

You may also place your order by telephone or if you have an NTIS Deposit Account or an American Express card order through TELEX. The order desk number is (703) 557-4650 and the TELEX number is 89-9405.

Thank you for your interest in NTIS. We appreciate your order.

METHOD OF PAYMENT

- ☐ Charge my NTIS deposit account no. _____
- ☐ Purchase order no. _____
- ☐ Check enclosed for $_____
- ☐ Bill me. Add $5.00 per order and sign below. (Not available outside North American continent.)
- ☐ Charge to my American Express Card account number

Card expiration date_____

Signature _____

☐ Airmail Services requested

NAME_____

ADDRESS_____

CITY. STATE. ZIP_____

Item Number	Quantity		Unit Price*	Total Price*
	Paper Copy (PC)	Microfiche (MF)		

All prices subject to change. The prices above are accurate as of 4/77

Foreign Prices on Request.

Sub Total	
Additional Charge	
Enter Grand Total	

Clip and mail to:

NTIS

National Technical Information Service
U.S. DEPARTMENT OF COMMERCE
Springfield, Va. 22161
(703) 557-4650 TELEX 89-9405